Inorganic Chemistry

Article

pubs.acs.org/IC

$Y(IO_3)_3$ as a Novel Photocatalyst: Synthesis, Characterization, and Highly Efficient Photocatalytic Activity

Hongwei Huang,*[†] Ying He,[†] Ran He,[‡] Zheshuai Lin,[‡] Yihe Zhang,*[†] and Shichao Wang[§]

[†]National Laboratory of Mineral Materials, School of Materials Science and Technology, China University of Geosciences, Beijing 100083, P. R. China

[‡]Center for Crystal Research and Development and Laboratory of Photochemical Conversion and Optoelectronic Materials, Technical Institute of Physics and Chemistry, Chinese Academy of Sciences, Beijing 100190, China

[§]Department of Chemistry, Northwestern University, Evanston, Illinois 60208, United States

Supporting Information

ABSTRACT: Nonbonding layer-structured $Y(IO_3)_3$ was successfully prepared by a simple hydrothermal route and investigated as a novel photocatalyst for the first time. Its crystal structure was characterized by X-ray diffraction, high-resolution transmission electron microscopy, and scanning electron microscopy. The optical absorption edge and band gap of $Y(IO_3)_3$ have been determined by UV−vis diffuse reflectance spectra. Theoretical calculations of the electronic structure of $Y(IO_3)_3$ confirmed its direct optical transition property near the absorption edge region, and the orbital components of the conduction band and valence band (VB) were also analyzed. The photocatalytic performance of $Y(IO_3)_3$ was evaluated by photooxidative decomposition of rhodamine B under ultraviolet light irradiation. It demonstrated that $Y(IO_3)_3$ exhibits highly efficient photocatalytic activity, which is much better than those of commercial TiO_2 (P25) and important UV photocatalysts BiOCl and $BiIO_4$. The origin of the excellent photocatalytic performance of $Y(IO_3)_3$ was investigated by electron spin resonance and terephthalic acid photoluminescence techniques. The results revealed that the highly strong photooxidation ability that resulted from its very positive VB position should be responsible for the excellent photocatalytic performance.

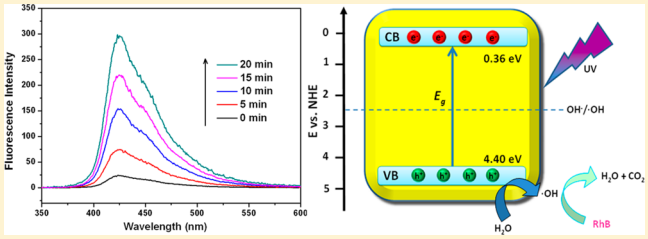

INTRODUCTION

Photocatalysis is expected to be a very meaningful and green technique for environmental purification and generation of clean energy.[1−3] Over the past several decades, numerous photocatalytic materials have been discovered.[4,5] Nevertheless, some photocatalysts show low activity, while others require rigorous synthetic conditions or have high toxicity. Thus, developing a new efficient photocatalyst is still a great challenge in the photocatalysis field. In particular, a photocatalyst with a very positive valence band (VB) position will have very strong photooxidation ability for the elimination of contaminants.

Recently, the non-metal oxy-acid salts were found to be a good source for exploration of new photocatalysts with strong photocatalytic ability to decompose organic contaminants. These new types of photocatalytic materials mainly include phosphates,[6−9] borates,[10,11] nitrates,[12,13] etc. In addition, the non-metal oxy-acid salt photocatalysts also possess advantages, such as broad sources, low cost, nontoxicity, etc. With regard to the benefits mentioned above, it may be a very promising way to explore new non-metal oxy-acid salts for the practically photocatalytic application. Lately, Wang et al. and our group reported that the iodate $BiIO_4$ can serve as a novel photocatalyst and exhibits excellent photocatalytic activity for dye photodegradation.[14−17] Moreover, another iodate $Bi(IO_3)_3$ has also been found to be a photocatalysis active material.[16] As the main building unit in iodates, the $(IO_3)^-$ anion group is always polarized because of the lone pair electrons of I^{5+}. Meanwhile, these lone pair electrons favor the formation of a layered structure of crystals. The layered structure and polarization are very beneficial for the separation of photogenerated electrons (e^-) and holes (h^+).[10,18] Therefore, iodates have become a kind of promising photocatalytic material.

In this work, the photocatalytic performance of another iodate, $Y(IO_3)_3$, was investigated for the first time, which was found also to possess a layered structure. This novel photocatalyst has been developed via a facile hydrothermal method. The photocatalytic activity of $Y(IO_3)_3$ was determined for the degradation of rhodamine B (RhB) under UV light irradiation. Moreover, electron spin resonance (ESR) and terephthalic acid photoluminescence (TA-PL) techniques were also employed to investigate the photocatalytic mechanism of $Y(IO_3)_3$.

EXPERIMENTAL SECTION

Synthesis Procedure. Raw materials are all analytic grade purity and used as received without further purification. $Y(IO_3)_3$ products were obtained via a hydrothermal approach. Typically, raw materials of

Received: May 16, 2014
Published: July 24, 2014

   dx.doi.org/10.1021/ic501127d | Inorg. Chem. 2014, 53, 8114−8119

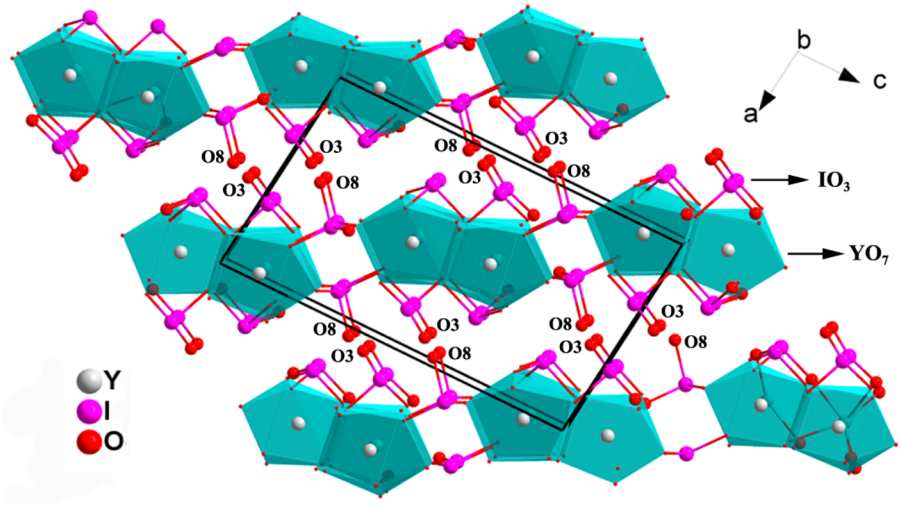

Figure 1. Crystal structure of $Y(IO_3)_3$.

$Y(NO_3)_3{\cdot}6H_2O$ and I_2O_5 in stoichiometric proportions were dissolved in 30 mL of distilled water while being stirred for 30 min to obtain a homogeneous solution. Afterward, the resulting mixture was transferred in a Teflon-lined autoclave and heated at 180 °C for 24 h. The final products were subsequently filtrated, washed several times with distilled water and ethanol, and then dried at 80 °C for 4 h.

The BiOCl and $BiIO_4$ reference samples were prepared by the methods previously reported in the literature.[16,18]

Characterization. The crystal structures of as-synthesized samples were characterized by X-ray diffraction (XRD) in a Cu Kα-radiated Bruker D8 ADVANCE X-ray diffractometer. The microstructure and morphology of $Y(IO_3)_3$ were researched by using scanning electron microscopy (SEM) (model S-4800), transmission electron microscopy (TEM), and high-resolution transmission electron microscopy (HRTEM) (model JEM-2100F). UV−visible diffuse reflectance spectra (DRS) were recorded with the aid of a Cary 5000 UV−visible−near infrared spectrophotometer. The Brunauer−Emmett−Teller (BET) surface areas of the four photocatalysts were obtained on the basis of the nitrogen adsorption method (Micromeritics 3020). Electron spin resonance (ESR) measurements of spin-trapped radical species were taken on an electron paramagnetic resonance spectrometer (EPR, ER200-SRC-10/12, Bruker).

Theoretical Calculations. The calculations performed on the electronic structures and densities of states (DOS) of $Y(IO_3)_3$ were conducted on the basis of the local density approximation (LDA), and the kinetic energy cutoff was set at 500 eV.[19,20] The total energy code CASTEP and planewave pseudopotential method were utilized.

Photocatalytic Evaluation. We evaluated the photocatalytic performance of $Y(IO_3)_3$ by decomposing RhB under ultraviolet light irradiation (an 300 W high-pressure lamp with a wavelength centered at 365 nm). The detailed procedures are as follows: 50 mg of photocatalyst was ultrasound-dispersed in 50 mL of an aqueous solution containing 10^{-5} mol/L RhB. Before irradiation, the dye and photocatalyst suspensions were stirred in the dark for 1 h. Then, these suspensions were exposed to UV light, and 4 mL of liquid was taken out at certain intervals and centrifuged. The RhB concentration was determined by recording the absorption spectra with an UV−vis spectrophotometer (Cary 5000).

Terephthalic Acid Fluorescence Probe. The hydroxyl radicals ($^{\bullet}OH$) can react readily with terephthalic acid (TA) to generate 2-hydroxyterephthalic acid (TAOH), which is a highly fluorescent product.[21] Thus, the amount of $^{\bullet}OH$ can be quantitatively determined by the intensity of TAOH. Via 315 nm excitation, TAOH emits fluorescence at ~425 nm. The photoluminescence (PL) spectra were recorded on a Hitachi F-4600 fluorescence spectrophotometer. The terephthalic acid fluorescence tests were conducted using procedures similar to those used for the photodegradation experiments described above, except RhB was replaced with TA.[22]

RESULTS AND DISCUSSION

Characterization on a Photocatalyst. Figure 1 depicts the crystal structure of $Y(IO_3)_3$, which crystallizes in monoclinic space group $P2/n$. The unit cell dimensions are as follows: a = 8.685(1) Å, b = 5.964(1) Å, and c = 14.958(1) Å.[23] In the asymmetric unit, there are only one crystallographically independent Y atom and three independent I atoms. The crystal structure of $Y(IO_3)_3$ is composed of (IO_3) anionic groups and YO_7 polyhedra. In the ionic groups, the Y−O and I−O distances range between 2.272(7) and 2.375(8) Å and between 1.792(9) and 1.823(0) Å, respectively. As shown in its structure, $Y(IO_3)_3$ exhibits an obviously layered structure along the {101} plane, and the $[IO_3]$ layers are stacked together by the nonbonding (van der Waals) interaction between the O3 and O8 atoms. As reported in the previous study, the layered crystal structure is very beneficial for the separation of photogenerated holes and electron pairs due to the strong internal electric field.

The X-ray powder diffraction (XRD) pattern of the as-obtained $Y(IO_3)_3$ sample is shown in Figure 2. We see that the experimentally obtained XRD pattern of $Y(IO_3)_3$ can closely match that from the Inorganic Crystal Structure Database (ICSD), and all the observed diffraction peaks can be indexed well into monoclinic $Y(IO_3)_3$. Moreover, no diffraction peaks

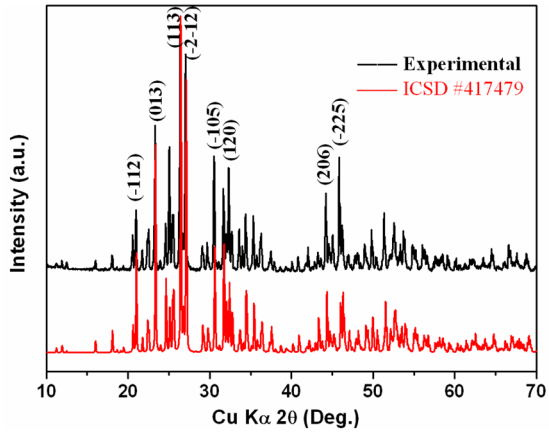

Figure 2. XRD pattern of $Y(IO_3)_3$.

dx.doi.org/10.1021/ic501127d | Inorg. Chem. 2014, 53, 8114−8119

for impurity were observed. These results demonstrate the successful synthesis of $Y(IO_3)_3$ with the pure phase.

The morphology and crystal size of the $Y(IO_3)_3$ photocatalyst were observed by scanning electron microscopy (SEM). It can be seen that $Y(IO_3)_3$ exhibits the morphology of a chunk structure, and the dimension of the blocks was ~2 μm (Figure S1 of the Supporting Information). The large size of the $Y(IO_3)_3$ product may be due to the relatively fast growth speed of the crystal seed. The obtained $Y(IO_3)_3$ sample was further characterized by HRTEM. The HRTEM image (Figure 3) and fast Fourier transform (FFT) images (inset of Figure 3)

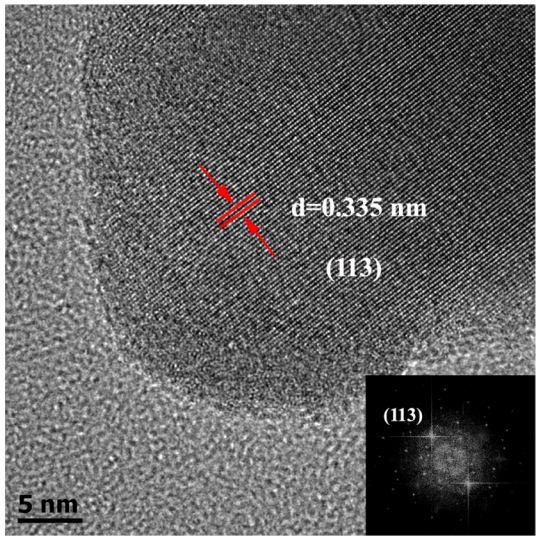

Figure 3. TEM and FFT (fast Fourier transition) pattern of the $Y(IO_3)_3$ sample.

demonstrate that the observed lattice spacing of the $Y(IO_3)_3$ crystal is 0.335 nm. This value is consistent with the spacing of the (113) plane of monoclinic $Y(IO_3)_3$.

Figure 4 shows the UV–vis diffuse reflectance spectrum of $Y(IO_3)_3$. We can see that the UV absorption edge of $Y(IO_3)_3$ is located at ~330 nm. The band gaps of $Y(IO_3)_3$ can be obtained through the following formula:

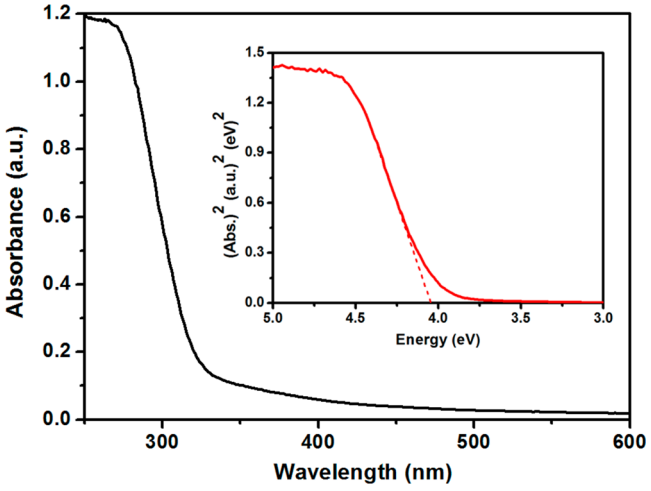

Figure 4. UV–vis diffuse reflectance spectra and band gap (inset) of $Y(IO_3)_3$.

$$\alpha h\nu = A(h\nu - E_g)^{n/2} \quad (1)$$

where parameters α, E_g, $h\nu$, and A are the absorption coefficient, band gap, photonic energy, and a constant, respectively. In eq 1, n is determined by the type of optical transition found in semiconductors (n values of 1 and 4 for direct and indirect absorption, respectively). For direct transitions, the square of the absorption coefficient is linear with energy, whereas the square root of the absorption coefficient is linear with respect to energy for indirect transitions.[24] The inset of Figure 4 shows that data plots of absorption^2 versus energy for $Y(IO_3)_3$ are nearly linear, demonstrating the direct transition property of its absorption edge (n = 1). Accordingly, the band gap of $Y(IO_3)_3$ was estimated to be 4.04 eV from the plot of absorption^2 versus energy. Besides, the conduction band (CB) and valence band (VB) positions can also be calculated by the following equations:[25]

$$E_{VB} = X - E^e + 0.5E_g \quad (2)$$

$$E_{CB} = E_{VB} - E_g \quad (3)$$

where E_g is the band gap, E^e is defined as the energy of free electrons on the hydrogen scale (~4.5 eV), and X is the absolute electronegativity of the semiconductor (geometric mean of the absolute electronegativity of the constituent atoms). The corresponding VB and CB levels of $Y(IO_3)_3$ were calculated to be 4.40 and 0.36 eV, respectively.

Band Structures and Density of States. The ab initio density functional theory (DFT) calculations were employed to study the calculated band structure of $Y(IO_3)_3$, which is displayed in Figure 5a. It can be found that the lowest unoccupied and highest occupied states are all located at point B. This observation verified that $Y(IO_3)_3$ is a direct bandgap semiconductor, which is in agreement with the evidence revealed by the UV–vis spectrum. In its band structure, the energy gap between the CB minimum and VB maximum is 2.8 eV, which is smaller than the actual value obtained from the optical absorption spectrum. The results are consistent with the fact that the band gap from DFT calculations is usually underestimated.

The corresponding partial density of states (PDOS) and total density of states (TDOS) of $Y(IO_3)_3$ are shown in Figure 5b. The bottom of the lowest unoccupied band is mainly composed of hybridized I 5p and O 2p orbitals; beyond that, the contribution of the Y 4d orbital was observed. Different from CB, most of the highest occupied band corresponding to VB is found to be composed of O 2p orbitals, which is the same with those in other oxides or oxygen compounds.[26–29]

Photocatalytic Performance. The photocatalytic performance for photodecomposing RhB over the investigated samples is shown in Figure 6a. The important UV photocatalysts TiO_2 (P25), BiOCl, and $BiIO_4$ are included as references. From Figure 6, the blank experiment (without photocatalysts) shows that RhB molecules are very stable and photolysis is negligible. RhB can be photodegraded by $Y(IO_3)_3$, $BiIO_4$, BiOCl, and TiO_2 in 6, 10, 12, and 16 min, respectively. It can be seen that $Y(IO_3)_3$ exhibits the highest decomposition efficiency of the four photocatalysts. To study the products of photodegradation of RhB, we performed high-performance liquid chromatography (HPLC). Figure S2 of the Supporting Information shows the HPLC spectra of the products generated during the photocatalytic degradation of RhB over YIO_3. It can

dx.doi.org/10.1021/ic501127d | Inorg. Chem. 2014, 53, 8114–8119

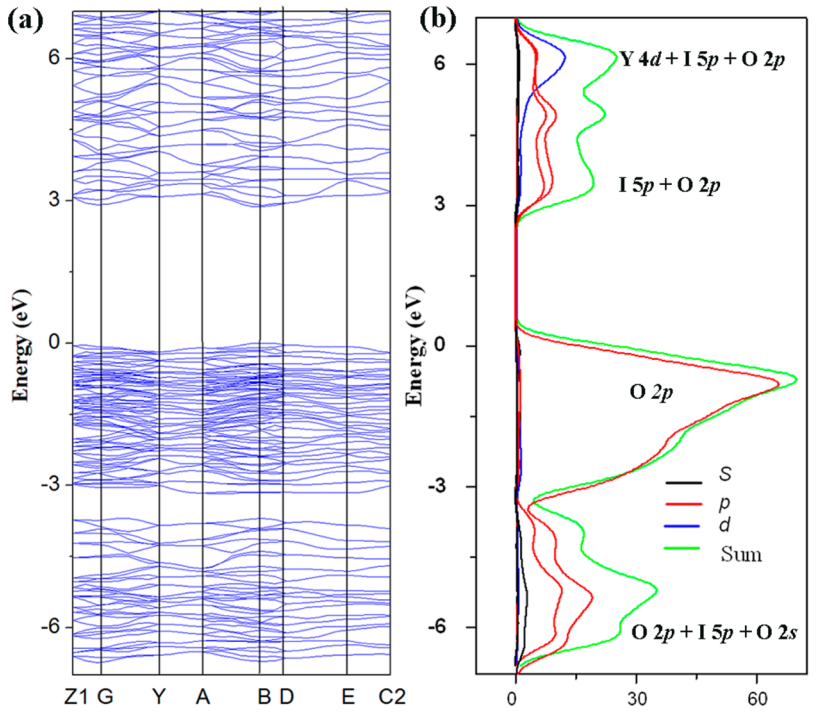

Figure 5. Band structure and density of states (DOS) of $Y(IO_3)_3$.

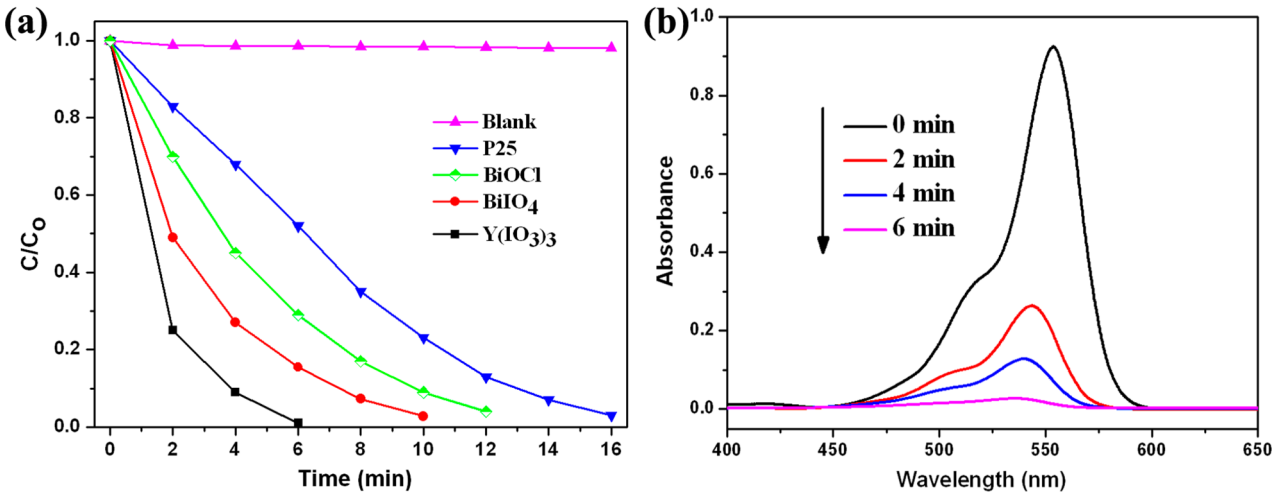

Figure 6. (a) Photocatalytic degradation curves of RhB over $Y(IO_3)_3$, $BiIO_4$, BiOCl, and TiO_2 (P25) under the irradiation of UV light. (b) Temporal absorption spectral patterns of RhB during the photodegradation process.

be found that there is no peak observed, indicating that RhB has been degraded to some small molecules, which cannot be detected by HPLC. Moreover, the apparent pseudo-first-order model according to the Langmuir–Hinshelwood (L–H) kinetics was employed to quantitatively understand the reaction kinetics of decomposition of RhB (Figure S3 of the Supporting Information). The corresponding k_{app} values determined from the experimental data described above are 0.614, 0.321, 0.203, and 0.113 for $Y(IO_3)_3$, $BiIO_4$, BiOCl, and TiO_2 (P25), respectively. Qualitative analysis indicated that the photocatalytic efficiency of $Y(IO_3)_3$ is approximately 5.4 times higher than that of P25, though the BET surface area of $Y(IO_3)_3$ (0.77 m^2/g) is only 1.5% of that of P25 (50 m^2/g). Figure 6b shows that the maximal absorbance of RhB molecules at 554 nm obviously decreases with an increase in irradiation time. The shift observed from 554 to 530 nm demonstrates the occurrence of de-ethylation and N-demethylation processes in the photochemical reaction.[30]

Mechanism of Photocatalytic Activity. Under UV light irradiation, the separation of photogenerated electron (e^-) and hole (h^+) pairs occurred, as illustrated in Figure 7. On the basis of the preceding band gap discussion, the holes in the VB of $Y(IO_3)_3$ possess a potential (4.40 eV) much more positive than that of $OH^-/{}^{\bullet}OH$ (1.99 eV vs the normal hydrogen electrode).[21] Thus, it could oxidize OH^- to generate abundant active ${}^{\bullet}OH$ radicals with powerful oxidization.

To determine the correctness of the mechanism, ESR spectroscopy was employed to detect the photogenerated radicals in the photocatalytic processes. We utilized BMPO as a spin trapping reagent of superoxide and hydroxyl radical. As shown in Figure 8, no characteristic ESR signal was detectable for the sample without irradiation. Under UV light irradiation,

dx.doi.org/10.1021/ic501127d | Inorg. Chem. 2014, 53, 8114–8119

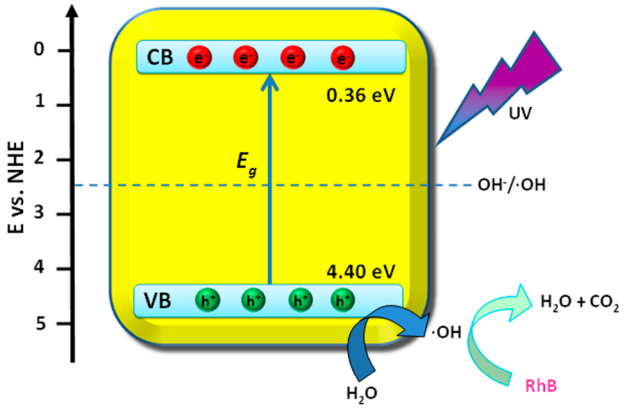

Figure 7. Photocatalytic mechanism of $Y(IO_3)_3$ under UV light irradiation.

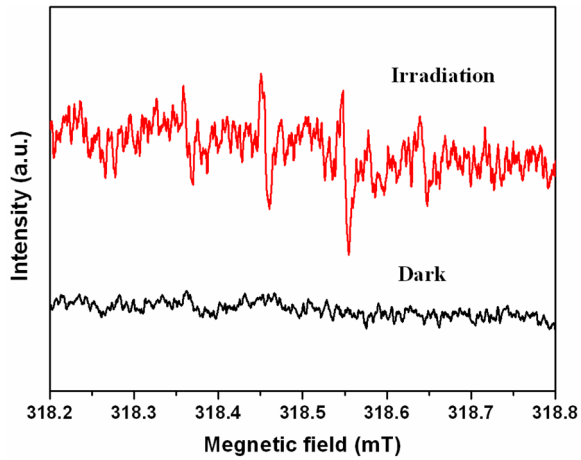

Figure 8. EPR spectra of $Y(IO_3)_3$ under UV light irradiation (DMPO as the radical trapper).

four peaks were clearly observed, which is the characteristic spectrum for the BMPO−•OH adduct in water,[31] indicating that •OH is the active species in the decomposition of RhB over $Y(IO_3)_3$.

To quantitatively reflect the amount of •OH radicals generated in this photocatalytic process, the terephthalic acid photoluminescence (TA-PL) method was employed. Figure 9 displays the fluorescence intensity of TAOH under UV light irradiation for 20 min. With a prolonged irradiation time, it is obvious that the rate of generation of •OH radicals gradually increases. The ESR and TA-PL results demonstrate that the •OH radicals serving as active species play crucial roles in the photodecomposition of RhB over $Y(IO_3)_3$. Moreover, $Y(IO_3)_3$ holds the most positive VB potential among the four photocatalysts, as revealed in Table 1. That may account for the highest photocatalytic activity of $Y(IO_3)_3$, though it possesses the smallest BET specific surface.

CONCLUSION

In summary, a novel photocatalyst $Y(IO_3)_3$ has been successfully prepared by a facile hydrothermal method. The results indicate that $Y(IO_3)_3$ exhibits obviously superior photocatalytic activity for decomposing RhB versus P25, and the important UV photocatalysts BiOCl and $BiIO_4$. The excellent photocatalytic performance of $Y(IO_3)_3$ should be ascribed to the its very positive VB position, which endows it with a highly strong photooxidation ability to produce abundant •OH radicals as active species for the efficient decomposition of RhB. It was verified by ESR and TA-PL tests.

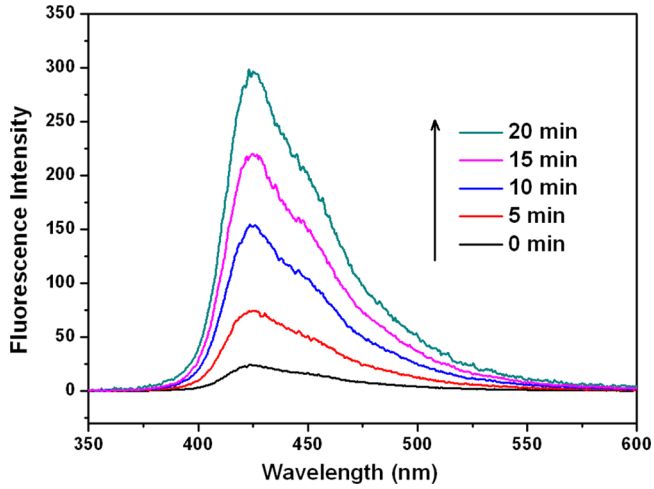

Figure 9. Changes in the fluorescence spectra of the irradiated $Y(IO_3)_3$ suspension containing 4 mM disodium terephthalate during various irradiation periods.

Table 1. Comparison of $Y(IO_3)_3$, $BiIO_4$, BiOCl, and P25

	$Y(IO_3)_3$	$BiIO_4$	BiOCl	P25
E_g (eV)	4.04	2.94	3.45	3.2
CB (eV)	0.36	0.87	0.23	−0.5
VB (eV)	4.40	3.81	3.68	2.7
S_{BET} (m^2/g)	0.77	2.35	8.34	48.6
K_{app}	0.614	0.321	0.203	0.113

ASSOCIATED CONTENT

Supporting Information

SEM image of $Y(IO_3)_3$ and HPLC spectrum and apparent rate constants for the photodegradation of RhB over $Y(IO_3)_3$, $BiIO_4$, BiOCl, and TiO_2 (P25). This material is available free of charge via the Internet at http://pubs.acs.org.

AUTHOR INFORMATION

Corresponding Authors

*E-mail: hhw@cugb.edu.cn.
*E-mail: zyh@cugb.edu.cn.

Notes

The authors declare no competing financial interest.

ACKNOWLEDGMENTS

This work was supported by the National Natural Science Foundation of China (Grant 51302251), Fundamental Research Funds for the Central Universities (2652013052), and the special co-construction project of the Beijing city education committee, Key Project of Chinese Ministry of Education (107023).

REFERENCES

(1) Kubacka, A.; Fernández-García, M.; Colón, G. *Chem. Rev.* **2012**, *112*, 1555−1614.
(2) Chen, X.; Mao, S. S. *Chem. Rev.* **2007**, *107*, 2891−2959.
(3) Shang, L.; Bian, T.; Zhang, B.; Zhang, D. H.; Wu, L. Z.; Tung, C. H.; Yin, Y. D.; Zhang, T. R. *Angew. Chem., Int. Ed.* **2014**, *53*, 250−254.

(4) Tong, H.; Ouyang, S. X.; Bi, Y. P.; Umezawa, N.; Oshikiri, M.; Ye, J. H. *Adv. Mater.* **2012**, *24*, 229−251.
(5) Liu, G.; Niu, P.; Yin, L. C.; Cheng, H. M. *J. Am. Chem. Soc.* **2012**, *134*, 9070−9073.
(6) Yi, Z. G.; Ye, J. H.; Kikugawa, N.; Kako, T.; Ouyang, S. X.; Stuart-Williams, H.; Yang, H.; Cao, J. Y.; Luo, W. J.; Li, Z. S.; Liu, Y.; Withers, R. L. *Nat. Mater.* **2010**, *9*, 559−564.
(7) Pan, C. S.; Zhu, Y. F. *Environ. Sci. Technol.* **2010**, *44*, 5570−5574.
(8) Huang, H. W.; Chen, G.; Zhang, Y. H. *Inorg. Chem. Commun.* **2014**, *44*, 46−49.
(9) Huang, H. W.; Chen, G.; Wang, S. B.; Kang, L.; Lin, Z. S.; Zhang, Y. H. *Mater. Res. Bull.* **2014**, *51*, 455−459.
(10) Huang, H. W.; He, Y.; Lin, Z. S.; Kang, L.; Zhang, Y. H. *J. Phys. Chem. C* **2013**, *117*, 22986−22994.
(11) Fan, X. Y.; Zang, L.; Zhang, M.; Qiu, H. S.; Wang, Z.; Yin, J.; Jia, H. Z.; Shilie Pan, S. L.; Wang, C. Y. *Chem. Mater.* **2014**, *26*, 3169−3174.
(12) Xie, L. Y.; Wang, J. X.; Hu, Y. H.; Zhu, S. Y.; Zheng, Z. Y.; Weng, S. X.; Liu, P. *RSC Adv.* **2012**, *2*, 9881−9886.
(13) He, Y.; Zhang, Y. H.; Huang, H. W.; Tian, N.; Luo, Y. *Inorg. Chem. Commun.* **2014**, *40*, 55−58.
(14) Nguyen, S. D.; Yeon, J.; Kim, S. H.; Halasyamani, P. S. *J. Am. Chem. Soc.* **2011**, *133*, 12422−12425.
(15) Wang, W.; Huang, B.; Ma, X.; Wang, Z.; Qin, X.; Zhang, X.; Dai, Y.; Whangbo, M.-H. *Chem.—Eur. J.* **2013**, *19*, 14777−14780.
(16) Huang, H. W.; He, Y.; He, R.; Jiang, X. X.; Lin, Z. S.; Zhang, Y. H.; Wang, S. C. *Inorg. Chem. Commun.* **2014**, *40*, 215−219.
(17) Huang, H. W.; Wang, S. B.; Tian, N.; Zhang, Y. H. *RSC Adv.* **2014**, *4*, 5561.
(18) Zhang, K. L.; Liu, C. M.; Huang, F. Q.; Zheng, C.; Wang, W. D. *Appl. Catal., B* **2006**, *68*, 125−129.
(19) Payne, M. C.; Teter, M. P.; Allan, D. C.; Arias, T. A.; Joannopoulos, J. D. *Rev. Mod. Phys.* **1992**, *64*, 1045−1097.
(20) Clark, S. J.; Segall, M. D.; Pickard, C. J.; Hasnip, P. J.; Probert, M. J.; Refson, K.; Payne, M. C. *Z. Kristallogr.* **2005**, *220*, 567−570.
(21) Ye, L. Q.; Liu, J. Y.; Jiang, Z.; Peng, T. Y.; Zan, L. *Appl. Catal., B* **2013**, *142*, 1−7.
(22) Wang, X. J.; Wang, Q.; Li, F. T.; Yang, W. Y.; Zhao, Y.; Hao, Y. J.; Liu, S. J. *Chem. Eng. J.* **2013**, *234*, 361−371.
(23) Phanon, D.; Mosset, A.; Gautier-Luneau, I. *Solid State Sci.* **2007**, *9*, 496−505.
(24) Zhang, X.; Ai, Z. H.; Jia, F. L.; Zhang, L. Z. *J. Phys. Chem. C* **2008**, *112*, 747−753.
(25) Ohko, Y.; Hashimoto, K.; Fujishima, A. *J. Phys. Chem. A* **1997**, *101*, 8057−8062.
(26) Huang, H. W.; Yao, J. Y.; Lin, Z. S.; Wang, X. Y.; He, R.; Yao, W. J.; Zhai, N. X.; Chen, C. T. *Angew. Chem., Int. Ed.* **2011**, *50*, 9141−9144.
(27) Huang, H. W.; Yao, J. Y.; Lin, Z. S.; Wang, X. Y.; He, R.; Yao, W. J.; Zhai, N. X.; Chen, C. T. *Chem. Mater.* **2011**, *23*, 5457−5463.
(28) Zhao, S. G.; Zhang, J.; Zhang, S. Q.; Sun, Z. H.; Lin, Z. S.; Wu, Y. C.; Hong, M. C.; Luo, J. H. *Inorg. Chem.* **2014**, *53*, 2521−2527.
(29) Zhao, S. G.; Gong, P. F.; Bai, L.; Xu, X.; Zhang, S. Q.; Sun, Z. H.; Lin, Z. S.; Hong, M. C.; Chen, C. T.; Luo, J. H. *Nat. Commun.* **2014**, *5*, 4019.
(30) Huang, G.; Zhu, Y. *J. Phys. Chem. C* **2007**, *111*, 11952−11958.
(31) Jiang, J.; Zhang, L. Z.; Li, H.; He, W. W.; Yin, J. J. *Nanoscale* **2013**, *5*, 10573−10581.

dx.doi.org/10.1021/ic501127d | *Inorg. Chem.* 2014, 53, 8114−8119